Inorganic Chemistry
Article

Inorg. Chem. **2010**, *49*, 1017–1026 **1017**
DOI: 10.1021/ic901853p

Hydrosulfide (HS^-) Coordination in Iron Porphyrinates

Jeffrey W. Pavlik,[†] Bruce C. Noll,[†] Allen G. Oliver,[†] Charles E. Schulz,*[,‡] and W. Robert Scheidt*[,†]

[†]*Department of Chemistry and Biochemistry, University of Notre Dame, Notre Dame, Indiana 46556 and*
[‡]*Department of Physics, Knox College, Galesburg, Illinois 61401*

Received September 18, 2009

Recent reports of potential physiological roles of hydrogen sulfide have prompted interest in heme−sulfide interactions. Heme−H_2S and/or heme−HS^- interactions could potentially occur during endogenous production, transport, signaling events, and catabolism of H_2S. We have investigated the interaction of the hydrosulfide ion (HS^-) with iron porphyrinates. UV−vis spectral studies show the formation of $[Fe(Por)(SH)]^-$, $[Fe(Por)(SH)_2]^{2-}$, and the mixed-ligand species $[Fe(Por)(Im)(SH)]^-$. UV−vis binding studies of [Fe(OEP)] and [Fe(T-*p*-OMePP)] (OEP = octaethylporphyrinate; T-*p*-OMePP = tetra-*p*-methoxyphenylporphyrinate) with HS^- allowed for calculation of the formation constants and extinction coefficients of mono- and bis-HS^- complexes. We report the synthesis of the first HS^--bound iron(II) porphyrin compounds, $[Na(222)][Fe(OEP)(SH)]\cdot 0.5C_6H_6$ and $[Na(222)][Fe(T\text{-}p\text{-}OMePP)(SH)]\cdot C_6H_5Cl$ (222 = Kryptofix-222). Characterization by single-crystal X-ray analysis, mass spectrometry, and Mössbauer and IR spectroscopy is all consistent with that of known sulfur-bound high-spin iron(II) compounds. The Fe−S distances of 2.3929(5) and 2.3887(13) Å are longer than all reported values of $[Fe^{II}(Por)(SR)]^-$ species. An analysis of the porphyrin nonplanarity for these derivatives and for all five-coordinate high-spin iron(II) porphyrinate derivatives with an axial anion ligand is presented. In our hands, attempts to synthesize iron(III) HS^- derivatives led to iron(II) species.

Introduction

Hydrogen sulfide (H_2S) has recently been recognized as a third possible gasotransmitter, along with NO and CO, and may play a role in vasodilation, blood pressure regulation, and neurological health.[1−5] Previously known H_2S biology consisted of its malodor and ability to inhibit cytochrome *c* oxidase.[6] However, the interaction of H_2S with mitochondrial cytochrome *c* oxidase is concentration-dependent.[7] Endogenously produced H_2S has been linked to hippocampal long-term potentiation[8] as well as neurological disorders such as Down's Syndrome and Alzheimer's disease.[9] The prospect of suspended animation in animals and humans is yet another facet of H_2S biology. When mice were exposed to 80 ppm of H_2S, they had sequential drops in their metabolic rate and core body temperature, similar to that observed in animals during the onset of hibernation.[10] After H_2S treatment was stopped, vital signs returned to normal, and no long-term functional or behavioral abnormalities were observed. This has prompted speculation into the use of H_2S as a means to improving postsurgery and post-trauma recovery.[11]

H_2S is produced endogenously in mammals by two enzymes. Cystathionine γ-lyase is the primary source of physiological H_2S in the mammalian cardiovascular system[12] and cystathionine β-synthase (CBS) in the central nervous system.[13] The endogenous H_2S levels in mammalian tissues is about 15 nM,[2] allowing for localized high intracellular gas concentrations like those observed in NO signaling, wherein the tissue function is altered upon nanomolar fluctuations.[14] At the biological pH of 7.4, dissolved H_2S, $pK_a = 6.9$, is partially deprotonated; the HS^-/H_2S ratio is 3:1, so one or more sulfide species could act as ligands to receptor proteins. Neither the binding species nor the receptors for potential sulfide−protein interactions associated with the

*To whom correspondence should be addressed. E-mail: scheidt.1@nd.edu.

(1) Abe, K.; Kimura, H. *J. Neurosci.* **1996**, *16*, 1066.
(2) Furne, J.; Saeed, A.; Levitt, M. D. *Am. J. Physiol. Regul. Integr. Comp. Physiol.* **2008**, *295*, R1479.
(3) Olson, K. R.; Dombrowski, R. A.; Russell, M. J.; Doellman, M. M.; Head, A. K.; Whitfield, N. L.; Madden, J. A. *J. Exp. Biol.* **2006**, *209*, 4011.
(4) Hosoki, R.; Matsuki, N.; Kimurs, H. *Biochem. Biophys. Res. Commun.* **1997**, *237*, 527.
(5) Mustafa, A. K.; Gadalla, M. M.; Snyder, S. H. *Sci. Signal.* **2009**, *2*, re2.
(6) Wever, R.; Van Gelder, B. F.; Dervartanian, D. V. *Biochim. Biophys. Acta* **1975**, *387*, 189.
(7) Cooper, C. E.; Brown, G. C. *J. Bioenerg. Biomembr.* **2008**, *40*, 533.
(8) Billaut-Laden, I.; Allorge, D.; Crunelle-Thibaut, A.; Rat, E.; Cauffiez, C.; Chevalier, D.; Houdret, N.; Lo-Guidice, J.; Broly, F. *Toxicology* **2006**, *225*, 1.
(9) Kamoun, P. *Amino Acids* **2004**, *26*, 243.
(10) Blackstone, E.; Morrison, M.; Roth, M. B. *Science* **2005**, *308*, 518.
(11) Leslie, M. *Science* **2008**, *320*, 1155.
(12) Yang, G.; Wu, L.; Jiang, B.; Yang, W.; Qi, J.; Cao, K.; Meng, Q.; Mustafa, A.; Mu, W.; Zhang, S.; Snyder, S.; Wang, R. *Science* **2008**, *83*, 587.
(13) Eto, K.; Kimura, H. *J. Neurochem.* **2002**, *83*, 80.
(14) Simonsen, U.; Wadsworth, R. W.; Buus, N. H.; Mulvany, M. J. *J. Physiol.* **1999**, *316*, 271.

Published on Web 12/28/2009

aforementioned phenomena have been identified; however, reactions of H_2S with heme proteins have been investigated for quite some time.

In 1933, Keilin[15] reviewed the previous work on H_2S−heme−protein studies, starting with the 1866 report by Hoppe-Seyler[16] of a green compound that formed irreversibly upon contact of methemoglobin with H_2S in the presence of oxygen. Haurowitz[17] was able to obtain a molecule that he called "sulpho-hemoglobin" with an absorption band at 618 nm that is clearly a porphyrin-based compound. The irreversible product was later suggested to be sulfhemoglobin, wherein the elements of H_2S add across a $\beta-\beta$ double bond of a pyrrole.[18] Subsequent NMR studies more firmly established structures of the covalently modified sulfur-containing pyrrole of protoporphyrin IX.[19] This modified pyrrole chemistry accounts for reports of patients exhibiting green blood and reduced oxygen transport after ingestion of certain sulfur-containing compounds.[20]

Direct interaction of sulfide with the iron center is also known. In Keilin's 1933 paper,[15] he also presented data that demonstrated that a new red product could be formed by the anaerobic reaction of H_2S with methemoglobin; this is commonly believed to be a coordination complex of the iron(III) porphyrin with sulfide. Neuroglobin, a highly preserved heme enzyme that occurs throughout the human central nervous system, regulates oxygen, and perhaps sulfide as has been shown in vitro, to bind H_2S quite tightly.[21] However, the best-understood interactions of heme proteins with H_2S are found in marine organisms that inhabit sulfide-rich environments.[22]

The most studied of these systems are the proteins from the clam *Lucina pectinata*, which has several different gill hemoglobins, of which hemoglobin I in its ferric form binds sulfide. The function of HbI[23] is apparently sulfide delivery to a symbiotic sulfide-oxidizing bacterium. Kraus et al.[24] have measured electron paramagnetic resonance (EPR) spectra of the anaerobically formed complexes of H_2S with whale myoglobin (Mb) and *L. pectinata* hemoglobins I and II (HbI and HbII). The EPR spectra are consistent with low-spin iron(III) complexes. The crystal structure of HbI−sulfide was reported by Rizzi et al.[25] in 1996; however, the complete ligand identity and iron oxidation state cannot be verified from the 1.9-Å resolution data. A very recent report suggests that H_2S, at high concentrations, will reduce the ferric HbI species.[26] There are a few other reports of heme−protein−H_2S interactions in the literature. An optical spectral study of the gill tissue from the bivalve mollusk *Solemya velum* led Doeller et al. to conclude that, in this case, hemoglobin must be converted from the ferrous state to the ferric state prior to sulfide binding.[27] The giant hemoglobin of *Oligobrachia mashikoi* can transport oxygen and sulfide simultaneously.[28]

These intriguing results for heme proteins prompted us to investigate iron porphyrinates with the hydrosulfide anion as a possible ligand. We first note that transition-metal complexes with hydrosulfide or H_2S as a ligand are rare. English et al.[29] reported the synthesis of an iron(III) species [Fe(T-*p*-OMePP)(SH)] using $S + LiB(C_2H_5)_3H$ (an unusual source of HS^-). The room temperature X-ray structure revealed a single axial atom at 2.30 Å from iron but without any evidence for a hydrogen atom. There is, however, a report of a failure to reproduce this preparation.[30] Cai and Holm[31] reported the transient formation of a species they believed to be $[Fe^{III}(OEP)(SH)]$ from the reaction of H_2S and $[Fe^{III}(OEP)]_2O$. The identification was based on an observed ^1H NMR *meso*-hydrogen shift of −50.0 ppm, but the complex quickly reduced to $[Fe^{II}(OEP)]$. Also reported in this work was $[Fe_4S_4(LS_3)-S-Fe(OEP)]^{m-2}$, where LS_3 = 1,3,S-tris[(4,6-dimethyl-3-mercaptophenyl)thio]-2,4,6-tris(*p*-tolylthio)benzene(3−), which contains an Fe−S−Fe bridge and is an analogue of certain assimilatory sulfite and nitrite reductases. Other (nonbiological) transition-metal hydrosulfide complexes of known structure include $[RhCl(H)(SH)(P(Ph_3)_2]_2$ and $[IrCl(H)(SH)(CO)(P(Ph_3)_2]$,[32] $[Mn^{III}(oespz)(SH)]$,[33] $[Co(cyclam)(SH)]_n[ClO_4]_n$ and $[Ni(\mu\text{-}SH)(cyclam)]_2[Ni(SH)_2(cyclam)][ClO_4]$,[34] *trans*-$[Rh(SH)(CO)(P(Ph_3)_2]$,[35] and *trans*-$[M(SH)_2(dmpe)_2]$; M = Cr, Fe.[36] For H_2S, there are just six structures, all of which are ruthenium(II) complexes.[37−39] One of these, $[Ru(IMes)_2(CO)(H_2S)H_2]$, is

(15) Keilin, D. *Proc. R. Soc. London, Ser. B: Biol. Sci.* **1933**, *133*, 393.
(16) Hoppe-Seyler, F. *Zentralbl. Med. Wiss.* **1866**, *4*, 436.
(17) Haurowitz, F. *Z. Physiol. Chem.* **1926**, *151*, 130.
(18) (a) Berzofsky, J. A.; Peisach, J.; Blumberg, W. E. *J. Biol. Chem.* **1971**, *246*, 3367. (b) Berzofsky, J. A.; Peisach, J.; Horecker, B. L. *J. Biol. Chem.* **1972**, *247*, 3783.
(19) (a) Chatfield, M. J.; La Mar, G. N.; Lecomte, J. T. J.; Balch, A. L.; Smith, K. M.; Langry, K. C. *J. Am. Chem. Soc.* **1986**, *108*, 710. (b) Chatfield, M. J.; La Mar, G. N.; Kauten, R. J. *Biochemistry* **1987**, *26*, 6939.
(20) Wu, C.; Kenny, M. A. *Clin. Chem.* **1997**, *43*, 162.
(21) Brittain, T.; Yosaatmadja, Y.; Henty, K. *IUBMB Life* **2008**, *60*, 135.
(22) Weber, R. E.; Vinogradov, S. N. *Physiol. Rev.* **2001**, *81*, 569.
(23) The following abbreviations are used in this paper: HbI, hemoglobin I from *L. pectinata*; OEP, dianion of 2,3,7,8,12,13,17,18-octaethylporphyrin; T-*p*-OMePP, dianion of *meso*-tetra-*p*-methoxyphenylporphyrin; TPP; dianion of *meso*-tetraphenylporphyrin; TMP, dianion of *meso*-tetramesitylporphyrin; TpivPP, dianion of α,α,α,α-tetrakis(*o*-pivalamidophenyl)porphyrin; Proto IX DME, dianion of protoporphyrin IX; Por, generalized porphyrin dianion; 222, 1,10-diaza-4,7,13,16,21,24-hexaoxabicyclo[8.8.8]hexacosane; Im, generalized imidazole; HIm, imidazole; 2-MeHIm, 2-methylimidazole; 1-MeIm, 1-methylimidazole; 2-MeIm, 2-methylimidazolate; cyclam, 1,4,8,11-tetraazacyclotetradecane; oespz, 2,3,7,8,12,13,17,18-octakis(ethylsulfanyl)-5,10,15,20-tetraazaporphyrinate dianion; dmpe, 1,2-bis(dimethylphosphino)ethane; IMes, 1,3-bis(2,4,6-trimethylphenyl)imidazol-2-ylidene.
(24) Kraus, D. W.; Wittenberg, J. B.; Jing-Fen, L.; Peisach, J. *J. Biol. Chem.* **1990**, *265*, 16054.
(25) Rizzi, M.; Wittenberg, J. B.; Coda, A.; Ascenzi, P.; Bolognesi, M. *J. Mol. Biol.* **1996**, *258*, 1.
(26) Pietra, R.; Lewis, A.; Leon, R. G.; Casabona, G.; Kiger, L.; Yeh, S.; Fernandez-Alberti, S.; Marden, M. C.; Cadilla, C. L.; Lopez-Garriga, J. *Biochemistry* **2009**, *48*, 4881.
(27) Doeller, J. E.; Kraus, D. W.; Colacino, J. M.; Wittenberg, J. B. *Biol. Bull.* **1988**, *175*, 388.
(28) Numoto, N.; Nakagawa, T.; Kita, A.; Sasayama, Y.; Fukumori, Y.; Miki, K. *Proc. Natl. Acad. Sci. U.S.A.* **2005**, *102*, 14521.
(29) English, D. R.; Hendrickson, D. N.; Suslick, K. S.; Eigenbrot, C. W.; Scheidt, W. R. *J. Am. Chem. Soc.* **1984**, *106*, 7258.
(30) Balch, A. L.; Cornman, C. R.; Safari, N.; Latos-Grażyński, L. *Organometallics* **1990**, *9*, 2420.
(31) Cai, L.; Holm, R. H. *J. Am. Chem. Soc.* **1994**, *116*, 7177.
(32) Mueting, A. M.; Boyle, P.; Pignolet, L. H. *Inorg. Chem.* **1984**, *23*, 44.
(33) Ricciardi, G.; Bencini, A.; Belviso, S.; Bavaso, A.; Lelj, F. *J. Chem. Soc., Dalton Trans.* **1998**, 1985.
(34) Pleus, R. J.; Waden, H.; Saak, W.; Haase, D.; Pohl, S. *J. Chem. Soc., Dalton Trans.* **1999**, 2601.
(35) Gaffney, T. R.; Ibers, J. A. *Inorg. Chem.* **1982**, *21*, 2851.
(36) Arif, A. M.; Hefner, J. G.; Jones, R. A.; Koschmieder, S. U. *J. Coord. Chem.* **1991**, *23*, 13.
(37) Chatwin, S. L.; Diggle, R. A.; Jazzar, R. F.; MacGregor, S. A.; Mahon, M. F.; Whittlesey, M. K. *Inorg. Chem.* **2003**, *42*, 7695.
(38) Mudalige, D. C.; Ma, E. S.; Rettig, S. J.; James, B. R.; Cullen, W. C. *Inorg. Chem.* **1997**, *36*, 5426.
(39) Sellman, D.; Lechner, P.; Knoch, F.; Moll, M. *J. Am. Chem. Soc.* **1992**, *114*, 922.

air-stable and forms a 16-electron species $[Ru(IMes)_2(CO)(SH)_2]$ upon treatment with H_2S.[37]

We report the binding of HS^- to three iron(II) porphyrins, [Fe(OEP)], [Fe(T-*p*-OMePP)], and [Fe(TMP)], which was followed spectrophotometrically, as well as the reaction of $[Fe(TMP)(1\text{-}MeIm)_2]$ with HS^-. We have been able to synthesize iron(II) derivatives and report the crystal structures of two hydrosulfido iron(II) porphyrinates, $[Na(222)][Fe(OEP)(SH)]\cdot 0.5C_6H_6$ and $[Na(222)][Fe(T\text{-}p\text{-}OMePP)(SH)]\cdot C_6H_5Cl$; both are five-coordinate and high-spin. Attempts to synthesize analogous iron(III) compounds were unsuccessful; in our hands, HS^- reduces iron(III) porphyrinates. $[Na(222)][Fe(OEP)(SH)]\cdot 0.5C_6H_6$ was further characterized by far-IR, mass spectrometry, and Mössbauer analysis. Most aspects of the two iron(II) complexes are similar to those of other five-coordinate anionic iron(II) porphyrinates, and comparisons are provided.

Experimental Section

General Information. All manipulations for the preparation of the five-coordinate iron(II) porphyrin derivatives were carried out under argon using a double-manifold vacuum line, Schlenkware, and cannula techniques. Benzene and hexanes were distilled over sodium benzophenone. Chlorobenzene was stirred over concentrated sulfuric acid, washed with a dilute Na_2CO_3 solution, dried with Na_2SO_4, and then distilled over P_2O_5. Octaethylporphyrin (H_2OEP) was synthesized from formaldehyde and 3,4-diethylpyrrole.[40] [Fe(OEP)Cl] was prepared according to a modified Adler preparation,[41] and $[Fe(OEP)]_2O$ was prepared from [Fe(OEP)Cl]. $[Fe(T\text{-}p\text{-}OMePP)]_2O$ and [Fe(TMP)(OH)] were also prepared by the same general procedure. All other chemicals were used as received from Aldrich or Fisher.

Mössbauer measurements were performed on a constant-acceleration spectrometer from 4.2 to 300 K with an optional small field and in a 9 T superconducting magnet system (Knox College). Samples for Mössbauer spectroscopy were prepared by immobilization of the crystalline material in Apiezon M grease.

Anhydrous NaHS. Anhydrous sodium hydrosulfide was prepared by a method described in *Inorganic Substances Handbook* with minor modifications.[42] In a drybox, each side of a 1 g cube of sodium was shaved to a shiny surface. The resulting cube was cut in half, and each half was pressed into a 1.5-mm-thin sheet using a spatula. If the sheets are not sufficiently thin, the interior sodium may be inaccessible for the reaction. The sheets were loosely rolled around the spatula and placed in a Schlenk tube. At the Schlenk line, 15 mL of benzene was added, and the mixture was stirred under an H_2S atmosphere for 2 days. The head gas was replaced several times with fresh H_2S during the reaction. Benzene was removed under vacuum, and the white powder NaHS was collected and stored under inert conditions. Solid NaHS is sparingly soluble in benzene or chlorobenzene. At higher concentrations, dissolution of the NaHS−Kryptofix mixture in chlorobenzene required 24 h of stirring. The resulting solution had a light-blue tint, consistent with the possible presence of small amounts of polysulfide ions such as S_3^{2-}.

$[Na(222)][Fe(OEP)(SH)]\cdot 0.5C_6H_6$. Standard Schlenk procedures were followed. A total of 50 mg (0.04 mmol) of $[Fe(OEP)]_2O$ was placed in a Schlenk flask, to which 10 mL of benzene and 1.0 mL of ethanethiol was added. The mixture was stirred for 2 h at 60 °C and then 16 h at 25 °C. Benzene and ethanethiol were removed under vacuum. The flask containing a purple powder was transferred into a drybox, where 5 mg (0.09 mmol) of NaHS and 34 mg (0.09 mmol) of Kryptofix(222) were added. The flask was removed from the drybox, and Schlenk procedures were resumed. A total of 10 mL of benzene was added, followed by stirring at 60 °C for 1 h. The mother liquor was divided evenly between four 7-mm-i.d. glass tubes by cannula transfer. A layer of 7 mL of hexanes was added to each tube. The tubes were flame-sealed under a slight vacuum and stored in the dark. Hexagonal pill-shaped crystals were harvested after 3 weeks. Yields from the tube reactions were about 42%. Large-scale preparations were not attempted. For Mössbauer spectroscopy, the same procedure was followed except that the hexanes and mother liquor were mixed together to cause immediate precipitation of the product, which was recovered by filtration and drying under vacuum.

$[Na(222)][Fe(T\text{-}p\text{-}OMePP)(SH)]\cdot C_6H_5Cl$. To a Schlenk flask were added 40 mg (0.025 mmol) of $[Fe(T\text{-}p\text{-}OMePP)]_2O$, 12 mL of chlorobenzene, and 1.0 mL of ethanethiol. The mixture was stirred for 2 h at 60 °C and then 16 h at 25 °C. Chlorobenzene and ethanethiol were removed under vacuum. The flask containing a purple powder was transferred to a drybox, where 4.5 mg (0.08 mmol) of NaHS and 32 mg (0.09 mmol) of Kryptofix(222) were added. After removal of the flask from the drybox, Schlenk procedures were resumed and 12 mL of chlorobenzene was added. This slurry was stirred at near boiling for 1 h in an oil bath until a brown-green solution resulted. Stirring and heating were terminated, and the reaction vessel remained undisturbed in the oil bath for 40 h. Purple needle-like crystals were collected by filtration of the reaction solution and were washed with hexanes. The yield was approximately 30%.

X-ray Crystallographic Studies. For $[Na(222)][Fe(OEP)(SH)]\cdot 0.5C_6H_6$, a crystal was placed in inert oil to reduce air exposure and cut by a razor blade to $0.5 \times 0.4 \times 0.3$ mm. Crystal data were collected and integrated using a Bruker Apex system, with graphite-monochromated Mo Kα radiation ($\lambda = 0.701\,73$ Å) at 100 K (700 Series Oxford Cryostream). The program *SADABS*[43] was applied for absorption corrections. The structure was solved by direct methods in *SHELXS-97*.[43] All structures were refined using *SHELXL-97*.[43] All non-hydrogen atoms were found after successive full-matrix least-squares refinement cycles on F^2 and then refined with anisotropic thermal parameters. Most hydrogen-atom positions were idealized with a riding model and fixed thermal parameters [$U_{ij} = 1.2U_{ij(eq)}$ or $1.5U_{ij(eq)}$] for the atom to which they are bonded. The exceptions are the sulfur-bound hydrogen atoms, which were refined freely, with and without constraints for comparison. For $[Na(222)][Fe(T\text{-}p\text{-}OMePP)(SH)]\cdot C_6H_5Cl$, disorder was found in one peripheral *p*-methoxyphenyl group with two orientations and three ethylene groups of the 222; three positions of the chlorobenzene solvate around an inversion center were required for a complete description. The sulfur-bound hydrogen atom in this case was refined freely, without constraints.

Mass Spectroscopy. In a drybox, isolated crystals of $[Na(222)][Fe(OEP)(SH)]\cdot 0.5C_6H_6$ with a combined mass of ~1 mg were dissolved in 500 μL of tetrahydrofuran. The solution was drawn into an airtight syringe, removed from the drybox, and injected into a JEOL AX505HA triple-quadrupole mass spectrometer with electrospray sample ionization and time-of-flight detection. Both negative- and positive-ion-mode spectra were collected for m/z 0−2000.

IR Spectroscopy. IR spectra were collected on a Nicolet Nexus 670 FT-IR with 2 cm^{-1} resolution equipped with EZ

(40) Milgram, B. C.; Eskildsen, K.; Richter, S. M.; Scheidt, W. R.; Scheidt, K. A. *J. Org. Chem.* **2007**, *72*, 3941.

(41) (a) Adler, A. D.; Longo, F. R.; Kampus, F.; Kim, J. *J. Inorg. Nucl. Chem.* **1970**, *32*, 2443. (b) Buchler, J. W. In *Porphyrins and Metalloporphyrins*; Smith, K. M., Ed.; Elsevier Scientific Publishing: Amsterdam, The Netherlands, 1975; Chapter 5.

(42) Lidin, R. A. *Inorganic Substances Handbook*; Begel House Inc.: New York, 1996; p 284.

(43) Sheldrick, G. M. *Acta Crystallogr., Sect. A* **2008**, *A64*, 112.

Table 1. Brief Crystallographic Data and Data Collection Parameters

	[Na(222)][Fe(OEP)(SH)]·0.5C_6H_6	[Na(222)][Fe(T-*p*-OMePP)(SH)]·C_6H_5Cl
formula	$[C_{36}H_{45}FeN_4S]^-$, $[C_{18}H_{36}N_2NaO_6]^+$·0.5C_6H_6	$[C_{48}H_{37}FeN_4O_4S]^-$, $[C_{18}H_{36}N_2NaO_6]^+$·C_6H_5Cl
fw, amu	1060.21	1333.75
a, Å	21.9682(4)	12.3987(5)
b, Å	23.7269(4)	25.3197(10)
c, Å	24.1203(6)	21.7450(8)
β, deg	116.676(1)	95.392(2)
V, Å^3	11234.2(4)	6796.2(5)
space group	$P2_1/n$	$P2_1/n$
Z	8	4
D_c, g/cm^3	1.254	1.304
F(000)	4552	2808
μ, mm^{-1}	0.367	0.361
cryst dimens, mm	0.47 × 0.39 × 0.34	0.33 × 0.13 × 0.12
radiation (*λ̄*, Å)	Mo Kα, 0.710 73	Mo Kα, 0.710 73
temperature, K	100(2)	100(2)
total data collected	398 321	90 934
abs corrn	semiempirical from equivalents	semiempirical from equivalents
unique data	37 293 (R_{int} = 0.046)	11 972 (R_{int} = 0.044)
unique obsd data [$I > 2\sigma(I)$]	27 137	8963
refinement method	full-matrix least squares on F^2	full-matrix least squares on F^2
final *R* indices [$I > 2\sigma(I)$]	R1 = 0.0456, wR2 = 0.1118	R1 = 0.0691, wR2 = 0.1934
final *R* indices (all data)	R1 = 0.0761, wR2 = 0.1346	R1 = 0.0922, wR2 = 0.2164

Omnic ESP, version 5.2a, software. Mid-IR spectra were collected from KBr pellets and far-IR from CsI pellets. All pellets were prepared in a drybox and then analyzed immediately. The CsI pellet was analyzed again after 24 h of air exposure for [Na(222)][Fe(OEP)(SH)]·0.5C_6H_6. A far-IR spectrum was also collected on a similarly prepared, ^{57}Fe-enriched crystalline sample of [Na(222)][Fe(OEP)(SH)]·0.5C_6H_6.

UV−Vis Binding Studies. Binding studies of HS^- in the form of solutions of Na(222)HS were carried out by the reaction of [Fe(OEP)], [Fe(T-*p*-OMePP)], or [Fe(TMP)] in order to determine the stoichiometry, bonding constants, and spectral properties. Displacement reactions of [Fe(TMP)(1-MeIm)$_2$] with Na(222)HS were also performed. Complete experimental details are given in the Supporting Information.

Results

The interaction of the HS^- ion with iron(II) porphyrinates has been established by a series of UV−vis observations on solutions of iron(II) porphyrinates with varying amounts of added NaHS. These data were interpreted as demonstrating the formation of both five-coordinate $[Fe(Por)(SH)]^-$ and six-coordinate $[Fe(Por)(SH)_2]^{2-}$.

Two different five-coordinate $[Fe(Por)(SH)]^-$ derivatives have been crystallized and structurally characterized. Both are five-coordinate high-spin species with an axial hydrosulfide ligand. Brief crystallographic data and intensity information are given in Table 1. [Na(222)][Fe(OEP)(SH)]·0.5C_6H_6 crystallizes with two porphyrin anions, two sodium cryptand cations, and a benzene solvate molecule in the asymmetric unit of the structure. The independent porphyrinate anions in the asymmetric unit will be referred to as **1** and **2**. Thermal ellipsoid plots of the two anions are given in Figures 1 and S1 in the Supporting Information. A diagram of the contents of the asymmetric unit of the structure is given in Figure S2 in the Supporting Information. A similar five-coordinate species was also found for [Na(222)][Fe(T-*p*-OMePP)(SH)]·C_6H_5Cl, and a thermal ellipsoid plot of the porphyrinate anion is presented in Figure S3 in the Supporting Information. Complete lists of bond distances and angles for all species are given in the Supporting Information.

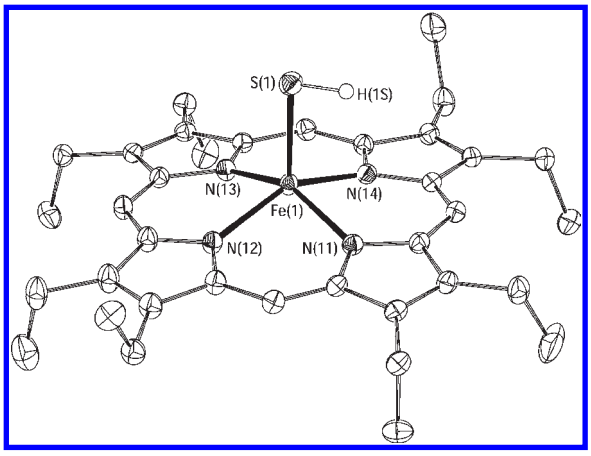

Figure 1. Thermal ellipsoid plot (50% probability ellipsoids) of anion **1** in [Na(222)][Fe(OEP)(SH)]·0.5C_6H_6 at 100 K. In this and other figures and tables, the following atom-naming convention has been used: *Q*(*n*), *Q*(*ny*), and *Q*(*nyy*), where *Q* is the atom type, *n* refers to anion **1** or **2**, and *y* and *yy* are further numbers and letters needed to completely specify the atom. Thus, similar atoms in the two anions have the same name except for the digit *n*. Hydrogen atoms (except where bound to sulfur) are omitted for clarity.

The OEP complex has also been characterized by electrospray mass, far-IR, and Mössbauer spectroscopy. As shown in Figure 2, the negative-ion-mode mass spectrum for [Na(222)][Fe(OEP)(SH)]·0.5C_6H_6 exhibits a series of peaks, *m*/*z* 619.3, 621.3, 622.3, and 623.3, with relative peak heights similar to those of the natural abundance isotopic distribution for $[Fe(OEP)(SH)]^-$, as shown by the red bars. Also shown in Figure 2 for comparison are the expected isotopic variant *m*/*z* and relative intensities for $[Fe(OEP)(Cl)]^-$ as blue bars. Mössbauer spectra for [Na(222)][Fe(OEP)(SH)], measured from 25 to 200 K, were consistent with the high-spin iron(II) state assigned to the complexes.

Discussion

Spectral Studies. The UV−vis spectra of [Fe^{II}(T-*p*-OMePP)] with varied concentrations of HS^- exhibit large spectral changes consistent with the formation of new

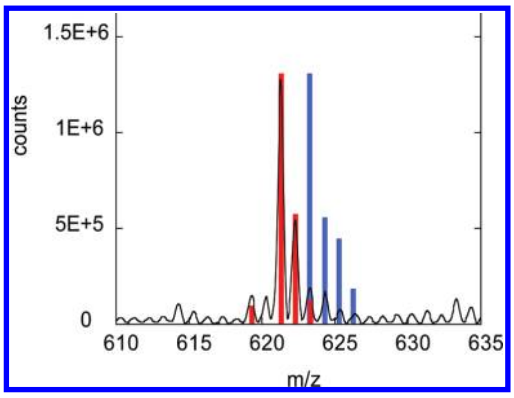

Figure 2. Negative-ion-mode mass spectrum of [Na(222)][Fe(OEP)(SH)] with overlays of calculated m/z, $z = 1$, for the four most abundant isotopic variants of $[Fe(OEP)(SH)]^-$ (red) and $[Fe(OEP)(Cl)]^-$ (blue). Bar heights are proportional to their calculated relative occurrence.

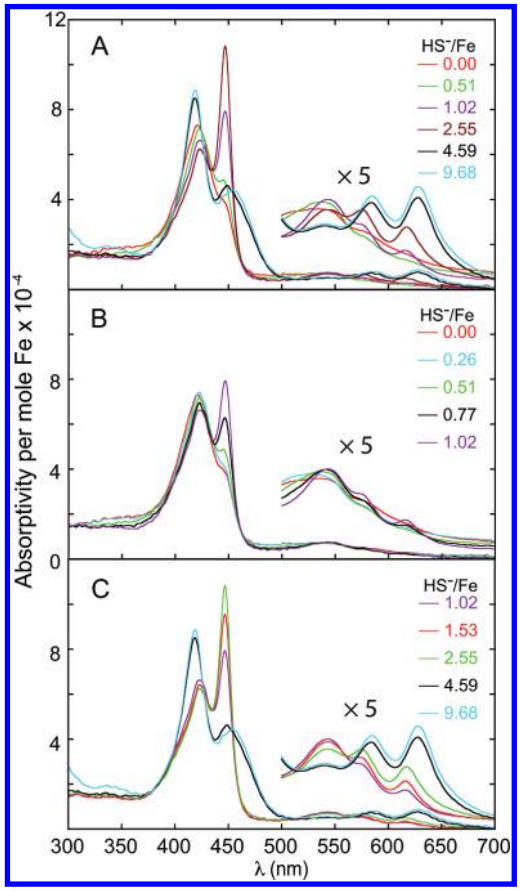

Figure 3. UV−vis molar absorptivity plots of chlorobenzene solutions of [Fe(T-*p*-OMePP)] with varied HS^-/Fe ratios. The concentration of [Fe(T-*p*-OMePP)] ranged from 0.085 to 0.073 mM, with the concentration of HS^- adjusted according to the ratios reported in the figure. A decrease in the [Fe(T-*p*-OMePP)] concentration is due to dilution incurred upon ligand addition. Panel A shows a selection of spectral traces from the complete range of HS^-/Fe ratios explored, panel B results from the lower HS^- concentrations, and panel C results from the highest HS^- concentrations. Note that, for reasons of clarity, the concentration color coding is distinct in each panel. From 500 to 700 nm, plots are shown at both regular scale and magnified 5×.

species. The complex changes are illustrated in the top panel (A) of Figure 3. The Soret peak at 420 nm in the initial spectrum has a modest shoulder at 444 nm. This shoulder markedly increases in intensity and becomes a sharp peak at 447 nm with maximum intensity at an HS^-/Fe ratio of near 2.5. The initial 420 nm peak drops substantially in intensity with increasing HS^- concentration until it has approximately half the intensity of the 447 peak and is slightly shifted to 423 nm at an HS^-/Fe ratio of near 2.5. Increasing HS^- concentrations lead to the final position of the Soret band at 419 nm along with a less intense band at 454 nm. The Q-band region for [Fe^{II}(T-*p*-OMePP)] displays commensurate spectral changes with increasing HS^- concentrations. The Q-band region starts with a broad peak at ~543 nm with two shoulders to the red. The shoulders gradually grow into resolved peaks at 584 and 628 nm at the highest HS^-/Fe ratios with intermediate peaks seen at 576 and 617 nm at a HS^-/Fe ratio of near 2.5. The initial peak at 543 nm decreases in intensity and shifts slightly to the red. The spectral changes over the lower and higher HS^- concentration ranges are shown as panels B and C, respectively, in Figure 3. These spectral changes clearly demonstrate that the reaction of [Fe^{II}(T-*p*-OMePP)] with HS^- leads to more than one new species. The two species are most probably identified as $[Fe^{II}(T\text{-}p\text{-}OMePP)(SH)]^-$ and $[Fe^{II}(T\text{-}p\text{-}OMePP)(SH)_2)]^{2-}$, as shown in the following equations.

$$[Fe^{II}(T\text{-}p\text{-}OMePP)] + HS^- \overset{K_1}{\rightleftharpoons} [Fe^{II}(T\text{-}p\text{-}OMePP)(SH)]^-$$

$$[Fe^{II}(T\text{-}p\text{-}OMePP)(SH)]^- + HS^- \overset{K_2}{\rightleftharpoons} [Fe^{II}(T\text{-}p\text{-}OMePP)(SH)_2]^{2-}$$

Formation constants were calculated using least-squares fits for the spectral data;[44] the data are summarized in Table 2.

The reaction of [Fe^{II}(OEP)] with HS^- gave equally complex spectra (shown in the top panel of Figure 4) and point to the formation of the same species as in the T-*p*-OMePP system. The broad Soret peak of [Fe^{II}(OEP)] at 384 nm splits into two sharper peaks as the HS^-/Fe ratio is increased from 0.0 to 1.5. Upon further ligand addition, the two Soret peaks at 384 and 410 nm coalesce into a single peak at 397 nm, which intensifies slightly at the highest HS^- levels. Further, a shoulder on the high-wavelength side of the Soret peak in the initial spectrum becomes gradually more prominent with increasing [HS^-] until in the limiting spectrum (HS^-/Fe ratio at 9.6) it is a nearly resolved peak at ~439 nm. The Q-band region again shows commensurate changes with increasing HS^- additions. The Q-band region in [Fe^{II}(OEP)] has two peaks at 529 and 562 nm. The lower-energy band intensifies to a maximum at a HS^-/Fe ratio of 1.5; the further addition of HS^- causes the two peaks to gradually coalesce into a single peak at 554 nm at the highest concentrations of HS^-. The spectral changes over the lower and higher HS^- concentration ranges are shown as panels B and C, respectively, in Figure 4. Formation

(44) Legget, D. J. SQUAD: Stability Quotients from Absorbance Data. In *Computational Methods for the Determination of Formation Constants*; Legget, D. J., Ed.; Modern Inorganic Chemistry Series; Plenum Press: New York, 1996; pp 159−217.

Table 2. Formation Constants and Derived λ_{max} (log ε) Values for Hydrosulfide Porphyrinate Complexes

		Soret[a]		Q band[a]		
complex	stability constant					
$[Fe(OEP)(SH)]^-$	5.0 ± 0.2^b	380 (4.84)	416 (5.03)	528 (4.07)	562 (4.21)	
$[Fe(OEP)(SH)_2]^{2-}$	10.4 ± 0.2^c	397 (4.89)		552 (4.17)		
$[Fe(T\text{-}p\text{-}OMePP)(SH)]^-$	4.7 ± 0.4^b	428 (4.81)	447 (5.10)	543 (4.07)	613 (3.55)	
$[Fe(T\text{-}p\text{-}OMePP)(SH)_2]^{2-}$	8.7 ± 0.4^c	418 (4.98)	459 (4.69)	585 (4.03)	627 (4.10)	
$[Fe(TMP)(SH)]^-$	4.6 ± 0.7^b	421 (5.36)	446 (5.10)	542 (4.38)	610 (3.76)	656 (3.64)
$[Fe(TMP)(SH)_2]^{2-}$	9.2 ± 0.4^c	416 (4.90)	452 (4.73)	584 (4.12)	627 (4.06)	

[a] nm. [b] log K_1, $K_1 = [Fe(Por)(SH)^-]/[Fe(Por)][SH^-]$. [c] log β_2, $\beta_2 = [Fe(Por)(SH)_2{}^{2-}]/[Fe(Por)][SH^-]^2$.

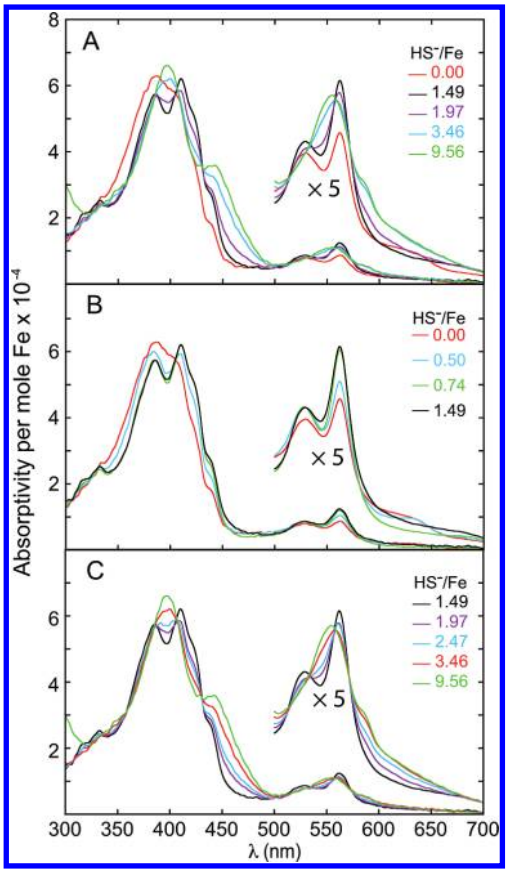

Figure 4. UV−vis molar absorptivity plots of chlorobenzene solutions of [Fe(OEP)] with varied HS^-/Fe ratios. The concentration of [Fe(OEP)] ranged from 0.113 to 0.088 mM, with the concentration of HS^- adjusted according to the ratios reported in the figure. The decrease in the [Fe(OEP)] concentration is due to dilution incurred upon ligand addition. Panel A shows a selection of spectral traces from the complete range of HS^-/Fe ratios explored, panel B results from the lower HS^- concentrations, and panel C results from the highest HS^- concentrations. Note that, for reasons of clarity, the concentration color coding is distinct in each panel. From 500 to 700 nm, plots are shown at both regular scale and magnified 5×.

constants were again calculated using least-squares fits for the spectral data, and values are summarized in Table 2. The spectral changes observed during the reaction of $[Fe^{II}(TMP)]$ with HS^- (given in Figure S4 of the Supporting Information) are quite similar to those of $[Fe^{II}(T\text{-}p\text{-}OMePP)]$, with only small differences in the wavelength maxima and relative intensities, as shown in Table 2.

The spectral changes observed in the reaction of $[Fe^{II}(TMP)(1\text{-}MeIm)_2]$ with HS^- also indicate the formation of a new species. When a solution of $[Fe^{II}(TMP)(1\text{-}MeIm)_2]$ was reacted with increasing levels of HS^-, a large increase of the Soret band is observed as the HS^-/Fe ratio is increased from 0.0 to 1.2, followed by a rapid decrease as the HS^-/Fe ratio is increased from 1.2 to 4.7. The limiting spectrum shown in Figure 5 is strikingly similar to the limiting spectrum from the reaction of $[Fe^{II}(TMP)]$ with HS^- (Figure S4 in the Supporting Information), consistent with a common final species. We suggest that the species responsible for the intense Soret peak at the HS^-/Fe ratio of 1.2 is $[Fe^{II}(TMP)(SH)(1\text{-}MeIm)]^-$ and that further additions of HS^- results in the formation of $[Fe^{II}(TMP)(SH)_2]^{2-}$.

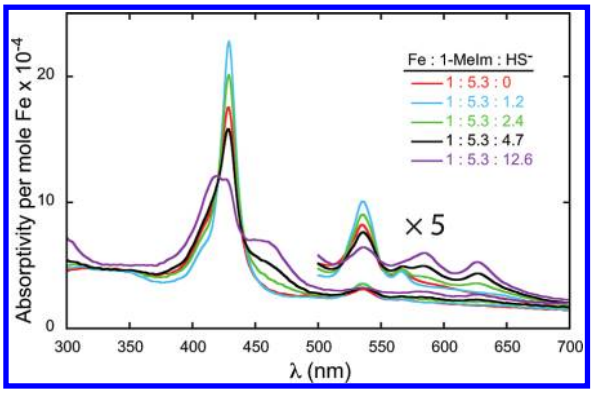

Figure 5. UV−vis molar absorptivity plots of chlorobenzene solutions of [Fe(TMP)] with varied Fe/1-MeIm/HS^- ratios. The concentration of [Fe(TMP)] ranged from 0.069 to 0.053 mM, while 1-MeIm ranged from 0.36 to 0.28 mM and HS^- was adjusted according to the ratios reported in the figure. The decrease in the [Fe(TMP)] concentration is due to dilution incurred upon ligand addition. From 500 to 700 nm, plots are shown at both regular scale and magnified 5×.

Synthesis. The strong evidence for the existence of $[Fe^{II}(Por)(SH)]^-$ and $[Fe^{II}(Por)(SH)_2]^{2-}$ led us to attempt their synthesis for further characterization. Crystallization experiments with the OEP and T-*p*-OMePP derivatives yielded crystals of the five-coordinate species, $[Na(222)][Fe^{II}(Por)(SH)]$, with the HS^-/Fe ratio ranging from 1.2 to 2.0 in the crystallizing solvent. Crystallization from solutions with the HS^-/Fe ratio of 5.0, near the solubility-imposed maximum, again yields the five-coordinate species. The lower solubility of the five-coordinate species, and/or instability of the doubly charged bis-HS^- adduct, may preclude isolation of $[Fe^{II}(Por)(SH)_2]^{2-}$ as a solid. Similar results were obtained for bulk preparations where only the five-coordinate species were obtained. All attempts to prepare mixed-ligand species were unsuccessful.

Attempts to prepare iron(III) species also were not successful; the HS^- ligand reduced all iron(III) porphyrinates used. In our attempts to prepare $[Fe^{III}(Por)(SH)]$

species, we reacted [Fe(Por)($OClO_3$)], Por = OEP or T-*p*-OMePP, with NaHS in chlorobenzene in the presence of (222) to aid in the solubilization of NaHS. In all cases, mixtures of $[Fe(Por)(SH)]^-$ and $[Fe(Por)(SH)_2]^{2-}$ were obtained. Spectra obtained from these synthetic procedures were similar to those obtained from the reaction of $[Fe^{II}(Por)]$ with HS^-, as shown in Figure S7 in the Supporting Information. This is in contrast to the earlier report of the preparation of the low-spin iron(III) derivative [Fe(T-*p*-OMePP)(SH)].[29] A certain ambiguity is associated with this complex because no direct evidence for the hydrogen atom of HS^- was obtained nor was an Fe−S stretch observed. However, the physical properties of [Fe(T-*p*-OMePP)(SH)] were consistent with an axially symmetric low-spin iron(III) species and include Mössbauer, EPR, NMR, and magnetic susceptibilities. The low-spin state seems unexpected. A reduction, but a rather slow reduction, of $[Fe^{III}$(T-*p*-OMePP)(SH)] on standing in a toluene or benzene solution was noted. It is possible that environmental factors play a significant role in this reduction. The apparent ease of reduction of iron(III) porphyrinates to iron(II) in reactions with hydrosulfide leads us to believe that the stability of the reported sulfide-bound iron(III) heme proteins results either from a specialized (low-polarity) protein environment or from the protein allowing only limited access to the binding site, which deters reduction at low concentrations of sulfide species.

Far-IR spectra gave $\nu_{Fe-S} = 344\ cm^{-1}$ in [Na(222)][Fe(OEP)(SH)]; the peak shifted to 340 cm^{-1} in the ^{57}Fe isotopomer, confirming the participation of iron in the vibration. The analogous peak in [Na(222)][Fe(T-*p*-OMePP)(SH)] was found at 337 cm^{-1}. Exposure of the original pellet to air for 24 h led to the disappearance of the 344 cm^{-1} Fe−S peak. The IR stretch of the SH group was not observed for either porphyrin complex; the band is typically weak but has been previously reported at 2550 cm^{-1} for $[Fe(SH)_2(dmpe)_2]$.[36] The electrospray mass spectrum, described earlier, clearly demonstrates that the axial ligand is not chloride, a common possible impurity in the iron(II) systems.

Mössbauer Spectra. Mössbauer spectra for $[Na(222)][Fe^{II}(OEP)(SH)]\cdot 0.5C_6H_6$ were collected between 25 and 200 K in a 500 G magnetic field. The spectra consist of two peaks that broaden with decreased temperature. Shoulders are clearly evident in the 25 K spectrum consistent with two quadrupole doublets, as shown in Figure 6. The data can be fit to four, equal area, overlapped Lorentzian lines for each temperature; values of the fits are provided in Table 3. The two quadrupole doublets are designated as "a" and "b". At 25 K, the quadrupole splitting (ΔE_Q) values are 2.81 and 2.14 mm/s with corresponding isomer shifts (δ_{Fe}) of 0.95 and 0.89 mm/s. Some temperature dependence was observed; ΔE_Q values are 2.62 and 2.09 mm/s with corresponding δ_{Fe} values of 0.92 and 0.89 mm/s at 200 K.

The observed ΔE_Q and δ_{Fe} values are strongly consistent with known high-spin iron(II) porphyrin complexes.[45] Isomer shift values are far too large to be

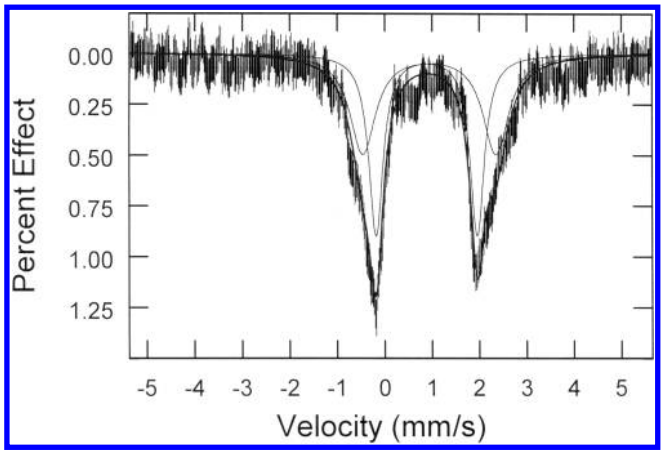

Figure 6. Mössbauer spectrum of $[Na(222)][Fe(OEP)(SH)]\cdot 0.5C_6H_6$ at 25 K with a magnetic field of 500 G. The experimental data and deconvolution of the spectrum into two equal-area doublets are shown.

Table 3. Mössbauer Parameters for $[Na(222)][Fe(OEP)(SH)]\cdot 0.5C_6H_6$

iron site	$\Delta E_Q{}^a$	$\delta_{Fe}{}^a$	Γ^b	T^c
a	2.81	0.95	0.66	25
a	2.86	0.96	0.68	50
a	2.62	0.90	0.58	100
a	2.62	0.92	0.52	200
b	2.14	0.89	0.36	25
b	2.13	0.90	0.37	50
b	2.13	0.93	0.37	100
b	2.09	0.89	0.38	200

[a] mm/s. [b] fwhm, mm/s. [c] K.

consistent with iron(III) species. Table 4 compares the Mössbauer parameters of iron sites "a" and "b" with other high-spin iron(II) porphyrinates, four-coordinate iron(II) species, and some iron(III) compounds.[46−56] The most comparable species are those with axial thiolates as the ligand; $[Fe^{II}(TpivPP)(SC_2H_5)]^-$ has $\Delta E_Q = 2.18$ mm/s and $\delta_{Fe} = 0.83$ mm/s and $[Fe^{II}(TpivPP)(SC_6HF_4)]^-$ has $\Delta E_Q = 2.38$ mm/s and $\delta_{Fe} = 0.83$ mm/s. Other iron(II) compounds, with nitrogen or oxygen as anionic axial ligands, have slightly higher δ_{Fe} values but significantly larger ΔE_Q values; some representative examples are $[Fe(TPP)(2\text{-}MeIm^-)]^-$ with $\Delta E_Q = 3.60$ mm/s and

(45) Debrunner, P. G. Mössbauer Spectroscopy of Iron Porphyrins. In *Iron Porphyrins*; Lever, A. B. P., Gray, H. B., Eds.; VCH Publishers Inc.: New York, 1983; Chapter 2, Part 3.

(46) Nasri, H.; Fischer, J.; Weiss, R.; Bill, E.; Trautwein, A. *J. Am. Chem. Soc.* **1987**, *109*, 2549.
(47) Schappacher, M.; Weiss, R. R.; Montiel-Montoya, R.; Gonser, U.; Bill, E.; Trautwein, A. *Inorg. Chim. Acta* **1983**, *78*, L9.
(48) Hu, C.; Noll, B. C.; Schulz, C. E.; Scheidt, W. R. *J. Am. Chem. Soc.* **2005**, *127*, 15018.
(49) Shaevitz, B. A.; Lang, G.; Reed, C. A. *Inorg. Chem.* **1988**, *27*, 4607.
(50) Bominaar, E. L.; Ding, X.; Gismelseed, A.; Bill, E.; Winkler, H.; Trautwein, A. X.; Nasri, H.; Fisher, J.; Weiss, R. *Inorg. Chem.* **1992**, *31*, 1845.
(51) Collman, J. P.; Hoard, L.; Kim, N.; Lang, G.; Reed, C. A. *J. Am. Chem. Soc.* **1975**, *97*, 2676.
(52) Hu, C.; Noll, B. C.; Schulz, C. E.; Scheidt, W. R. *Inorg. Chem.* **2007**, *46*, 619.
(53) Strauss, S. H.; Silver, M. E.; Long, K. M.; Thompson, R. G.; Hudgens, R. A.; Spartalian, K.; Ibers, J. A. *J. Am. Chem. Soc.* **1985**, *207*, 4207.
(54) Maricondi, C.; Straub, D. K.; Epstein, L. M. *J. Am. Chem. Soc.* **1972**, *94*, 4157.
(55) Moss, T. H.; Bearden, A. J.; Caughey, W. S. *J. Chem. Phys.* **1969**, *51*, 2624.
(56) Tang, S. C.; Koch, S.; Papaefthymiou, G. C.; Foner, S.; Frankel, R. B.; Ibers, J. A.; Holm, R. H. *J. Am. Chem. Soc.* **1976**, *98*, 2414.

Table 4. Mössbauer Parameters for Relevant Iron(II) and -(III) Porphyrinates

complex	ΔE_Q[a]	δ_{Fe}[a]	Γ[b]	T[c]	ref
Iron(II) Complexes					
$[Fe(OEP)(SH)]^-$, site "a"	2.82	0.95	0.66	25	tw[d]
$[Fe(OEP)(SH)]^-$, site "b"	2.13	0.89	0.36	25	tw[d]
$[Fe(TpivPP)(SC_2H_5)]^-$	+2.18[e]	0.83	0.30	4.2	48
$[Fe(TpivPP)(SC_6HF_4)]^-$	2.38	0.83	0.32	4.2	47
$[Fe(TpivPP)(Cl)]^-$	4.36	1.01	0.31	77	47
$[Fe(TPP)(OC_6H_5]^-$	+4.01[e]	1.03	0.25	4.2	49
$[Fe(TpivPP)(O_2CCH_3)]^-$	+4.25[e]	1.05	0.30	4.2	50
$[Fe(TpivPP)(OCH_3)]^-$	3.67	1.03	0.40	4.2	46
$[Fe(TpivPP)(OC_6H_5]^-$	3.90	1.06	0.38	4.2	46
$[Fe(OEP)(2\text{-}MeIm^-)]^-$	+3.71[e]	1.00	0.29	4.2	48
$[Fe(TPP)(2\text{-}MeIm^-)]^-$	+3.60[e]	1.00	0.33	4.2	48
[Fe(TPP)] ($I\bar{4}2d$)	1.51	0.52	NR[f]	4.2	51
[Fe(TPP)] ($P\bar{1}$)	2.21	0.57	NR[f]	20	52
[Fe(OEP)]	1.71	0.62	NR[f]	4.2	53
Iron(III) Complexes					
[Fe(TPP)(Cl)]	0.46	0.41	NR[f]	4.2	54
[Fe(TPP)(Br)]	0.72	0.45	NR[f]	4.2	54
$[Fe(OEP)(SC_6H_5)]$	0.31	0.49	NR[f]	4.2	56

[a] mm/s. [b] fwhm, mm/s. [c] K. [d] This work. [e] Sign of ΔE_Q experimentally defined. [f] Not reported.

$\delta_{Fe} = 1.00$ mm/s and $[Fe(TPP)(OC_6H_5)]^-$ with $\Delta E_Q = 4.01$ mm/s and $\delta_{Fe} = 1.03$ mm/s. Four-coordinate iron(II) compounds have significantly lower δ_{Fe} values, 0.52 and 0.62 mm/s for [Fe(TPP)] and [Fe(OEP)], respectively. Possible reasons for the appearance of two Mössbauer distinguishable sites in crystalline $[Na(222)][Fe^{II}(OEP)(SH)]\cdot 0.5C_6H_6$ will be discussed subsequently.

Structures of the $[Fe^{II}(Por)(SH)]^-$ Anions. The asymmetric unit of crystalline $[Na(222)][Fe^{II}(OEP)(SH)]\cdot 0.5C_6H_6$ contains two square-pyramidal anions with hydrosulfide as the axial anionic ligand, as shown in in Figures 1 and S1 in the Supporting Information. The two anions will be referred to as anion **1** and anion **2**. The two porphyrin moieties do have some small, but significant, differences in their coordination geometry. The average $Fe-N_p$ distances are consistent with high-spin iron(II) complexes: 2.1192(13) Å for anion **1** and 2.1081(14) Å for anion **2**.[57,58] The Fe−S distances of 2.3929(5) and 2.3830(5) Å for **1** and **2**, respectively, are reasonable, longer than the 2.340(5) Å Fe−Cl of $[Fe^{II}(TPP)(Cl)]^-$ [59] and shorter than the 2.434(2) Å Fe−Br of $[Fe^{II}(TpivPP)(Br)]^-$.[60] Known iron(II) thiolate values: 2.360(2) Å in $[Fe^{II}(TPP)(SC_2H_5)]^-$ [61] and 2.324(2) Å in $[Fe^{II}(TpivPP)(SC_2H_5)]^-$ [62] are slightly shorter than the Fe−SH values. These data are summarized in Table 5. Also included in the table are other $[Fe^{II}(Por)X]$ complexes with singly charged anionic ligands[63,64] and related $[Fe^{III}(Por)(SR)]$ complexes.[66,67]

The atom displacements of the iron and the core atoms from the 24-atom and 4-nitrogen-atom mean planes of $[Fe^{II}(OEP)(SH)]^-$ are given in Figures 7 (anion **1**) and S5 in the Supporting Information (anion **2**). Also displayed on these formal diagrams are the averaged values of the bond distance and angle in each of the cores; the agreement between the two cores is very good. The iron atom displacements from the four-nitrogen planes (ΔN_4) of 0.55 and 0.52 Å for **1** and **2**, respectively, are consistent with the iron(II) anionic complexes, notably 0.53 Å of $[Fe^{II}(TPP)(Cl)]^-$,[59] 0.49 Å of $[Fe^{II}(TpivPP)(Br)]^-$,[60] and 0.52 Å of $[Fe^{II}(TPP)(SC_2H_5)]^-$.[61]

Interestingly, the porphyrin core conformations of anions **1** and **2** of $[Fe^{II}(OEP)(SH)]^-$ have some substantial differences. The plots of the iron atom displacements from the two mean planes of Figures 7 and S5 in the Supporting Information clearly show that both anions have domed cores but otherwise differ in the patterns of atom displacements. Clearly additional, but distinct, distortions from nonplanarity are present in the two anions. The differences for the two anions in the asymmetric unit occur despite identical composition in a common lattice. The different types of distortions have been categorized as ruffling, doming, saddling, waving, and propellering and may be simultaneously present in a porphyrin core to varying degrees.[68,69] The deformations can be differentiated using the normal-coordinate structural decomposition (NSD) procedure, a method to calculate the contribution from each type of distortion.[70] The results from the NSD analysis for the two $[Fe^{II}(OEP)(SH)]^-$ anions along with a number of additional high-spin iron(II) porphyrinates coordinated by an anionic axial ligand are presented in Table 6. The table makes clear that, although both $[Fe^{II}(OEP)(SH)]^-$ anions have a substantial doming component, the differing distortion is that the anion core of **1** has a ruffling component, whereas the anion core of **2** has a large saddling component. The overall difference in the core conformations probably leads to the modest difference in the $Fe-N_p$ bond distances.

As has been noted previously, the Mössbauer spectrum of crystalline $[Na(222)][Fe^{II}(OEP)(SH)]\cdot 0.5C_6H_6$ displayed two overlapping quadrupole doublets. The most likely explanation for the two signals is that the conformational differences are driving modest differences in the electronic distribution that is revealed in the quadrupole splitting values. Although we have no way of unambiguously associating a particular conformation with the quadrupole splitting, we think that the anion with its slightly longer $Fe-N_p$ bond distances is to be associated

(57) Scheidt, W. R.; Reed, C. A. *Chem. Rev.* **1981**, *81*, 543.
(58) Scheidt, W. R. Systematics of Porphyrins and Metalloporphyrins. In *The Porphyrin Handbook*; Kadish, K. M., Smith, K. M., Guilard, R., Eds.; Academic Press: San Diego, CA, 2000; Vol. *3*, pp 72−73.
(59) Hu, C.; Sulok, C. D.; Paulat, F.; Lehnert, N.; Zatsman, A. I.; Hendrich, M. P.; Schulz, C. E.; Scheidt, W. R., manuscript in preparation.
(60) Nasri, H. Ph.D. Thesis, University of Louis Pasteur, Strasbourg, France, **1987**.
(61) Caron, C.; Mitschler, A.; Riviere, G.; Ricard, L.; Schappacher, M.; Weiss, R. *J. Am. Chem. Soc.* **1979**, *101*, 7401.
(62) Schappacher, M.; Ricard, L.; Weiss, R. R.; Montiel-Montoya, R.; Bill, E.; Trautwein, A. X. *Inorg. Chem.* **1989**, *28*, 4639.
(63) Nasri, H.; Ellison, M. K.; Shaevitz, B.; Gupta, G. P.; Scheidt, W. R. *Inorg. Chem.* **2006**, *45*, 5284.
(64) Mandon, D.; Ott-Woelfel, F.; Fischer, J.; Weiss, R.; Bill, E.; Trautwein, A. X. *Inorg. Chem.* **1979**, *101*, 2442.
(65) Tang, S. C.; Koch, S.; Papaefthymiou, G. C.; Foner, S.; Frankel, R. B.; Ibers, J. A.; Holm, R. H. *J. Am. Chem. Soc.* **1976**, *98*, 2414.
(66) Miller, K. M.; Strouse, C. E. *Acta Crystallogr., Sect. C* **1984**, *C40*, 1324.
(67) Miller, K. M.; Strouse, C. E. *Inorg. Chem.* **1984**, *23*, 2395.
(68) Scheidt, W. R.; Lee, Y. J. Recent Advances in the Stereochemistry of Metallotetrapyrroles. *Struct. Bonding* (*Berlin*) **1987**, *64*, 1−70.
(69) Shelnutt, J. A.; Song, X.; Ma, J.; Jia, A.; Jentzen, W.; Medforth, C. J. *Chem. Soc. Rev.* **1998**, *27*, 31.
(70) Sun, L.; Shelnutt, J. A. Program is available via the internet at http://jasheln.unm.edu.

Table 5. Selected Distances (Å) and Angles (deg) for Iron(II) Porphyrinates with Anionic Ligands

complex	$\langle Fe-N_p \rangle^{a,b}$	$Fe-L^b$	$Fe-S-R^c$	$\Delta N_4^{b,d}$	ref
		Iron(II) Complexes			
$[Fe(OEP)(SH)]^-$, Fe(1)	2.1192(13)	2.3929(5)	98.5(10)[e]	0.55	tw
$[Fe(OEP)(SH)]^-$, Fe(2)	2.1081(14)	2.3830(5)	100.2(15)[e]	0.52	tw
$[Fe(TpOMePP)(SH)]^-$	2.108(5)	2.3887(13)	106.(2)[e]	0.52	tw
$[Fe(TPP)(SC_2H_5)]^-$	2.096(4)	2.360(2)		0.52	61
$[Fe(TpivPP)(SC_2H_5)]^-$	2.074(10)	2.324(2)	106.64	0.44	62
$[Fe(TpivPP)(OC_6H_5)]^-$	2.114(2)	1.937(4)		0.56	46
$[Fe(TpivPP)(O_2CCH_3)]^-$	2.107(2)	2.034(3)		0.55	46
$[Fe(TpivPP)(NO_3)]^-$	2.070(16)	2.069(4)		0.42	63
$[Fe(TpivPP)\ (2\text{-}MeIm^-)]^-$	2.11(2)	2.002(15)		0.52	64
$[Fe(TPP)(Cl)]^-$	2.1161(11)	2.3400(5)		0.56	59
$[Fe(TpivPP)(Cl)]^-$	2.108(15)	2.301(2)		0.53	47
$[Fe(TpivPP)(Br)]^-$	2.094(3)	2.434(3)		0.49	60
$[Fe(TpivPP)(I)]^-$	2.079(2)	2.712(1)		0.40	60
		Iron(III) Complexes			
[Fe(T-*p*-OMePP)(SH)][f]	2.0155(19)	2.2928(27)	NA	0.33	29
$[Fe(Proto\ IX\ DME)(SC_6H_4NO_2)]$	2.064(18)	2.324(2)	100.4(2)	0.43	65
$[Fe(OEP)(SC_6H_5)]$	2.057(6)	2.299(3)	102.5(3)	0.47	66
$[Fe(TPP)(SC_6HF_4)]$	2.058(2)	2.298(5)	103.7	0.40	67

[a] Average $Fe-N_p$ distance. [b] Å. [c] deg. [d] Iron displacement from the four-nitrogen plane. [e] R = H. [f] Low spin.

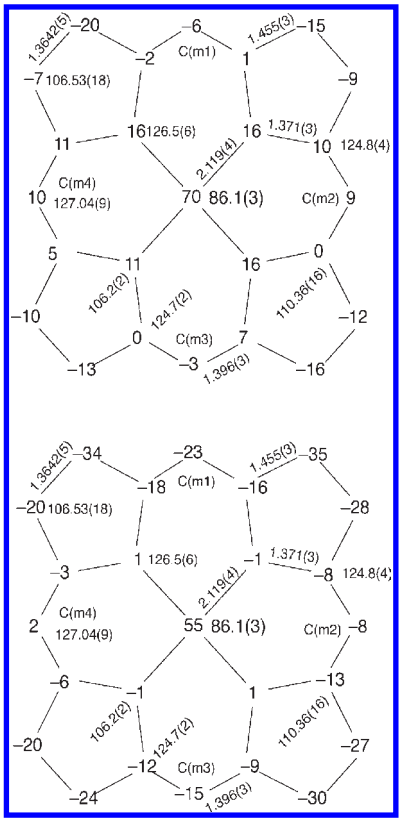

Figure 7. Mean-plane diagrams for anion **1** of [Na(222)][Fe(OEP)(SH)]·0.5C_6H_6. The values of the atomic displacements from 24-atom (top) and 4-nitrogen-atom (bottom) mean planes are given in units of 0.01 Å. Also entered on the diagrams are mean porphyrin core bond lengths in angstroms and mean bond angles in degrees.

with the larger quadrupole doublet ("a"). This issue is difficult to study because any rigorous evaluation requires samples with identical composition but differing core conformations. We carefully studied the crystal packing pattern to see if differing environments of the HS^- ligand could be the cause of the differing physical properties of the two anions. Significant differences are not apparent (see Figure S2 in the Supporting Information).

Table 6 also gives the results of the NSD analysis for a number of additional high-spin iron(II) porphyrinates with anionic axial ligands. All of these anionic species are seen to display significant core doming; moreover, all have at least one other significant core distortion mode. This is reflected in the large values of D_{oop} (a measure of the total displacements; Table 6). Note that none of these complexes are derivatives with peripheral crowding designed to induce significant nonplanar distortions. A similar analysis has been done for high-spin iron(II) porphyrinates with (neutral) imidazole as the axial ligand.[71] These two systems provide some interesting comparisons. Although the imidazole derivatives also frequently display core doming, the magnitude is, on average, only $^3/_4$ that of the anionic species. Moreover, the total distortion value D_{oop} is also only about 60% in the imidazole-ligated species. These differences are consistent with the idea that there are two distinct $S = 2$ states for high-spin iron porphyrinate derivatives that are characterized by, inter alia, apparent differences in the size of the iron center.[59]

The X-ray structure of a second hydrosulfide derivative, $[Fe(T\text{-}p\text{-}OMePP)(SH)]^-$, has also been determined. The coordination geometry for this complex is similar to that of its OEP analogue, with an Fe−S bond distance of 2.3887(13) Å and an average $Fe-N_p$ distance of 2.108(5) Å. Table 7 details the coordination site geometry, and Table 5 compares the geometry of $[Fe(T\text{-}p\text{-}OMePP)(SH)]^-$ to those of the OEP analogue and related porphyrin complexes. The displacements of all porphyrinate atoms from the 24-atom mean plane and the 4-nitrogen-atom plane are presented in Figure S6 in the Supporting Information. Although the porphyrin core is less domed

(71) See Table 3 of: Hu, C.; An, J.; Noll, B. C.; Schulz, C. E.; Scheidt, W. R. *Inorg. Chem.* **2006**, *45*, 4177.

Table 6. Out-of-Plane Displacements (Å) of the Minimal Basis for the X-ray Crystal Structures of Five-Coordinate High-Spin Iron(II) Porphyrinates

porphyrin	D_{oop}[a]	δ_{oop}[b]	*sad*	*ruf*	*dom*	*wav*(*x*)	*wav*(*y*)	*pro*	ΔN_4[c]	Δ[d]	ref
[Fe(OEP)(SH)]$^-$, Fe(1)	0.526	0.015	0.016	−0.207	−0.481	0.019	−0.014	0.035	0.55	0.70	tw
[Fe(OEP)(SH)]$^-$, Fe(2)	0.514	0.012	0.324	−0.001	−0.393	−0.049	0.041	−0.003	0.52	0.64	tw
[Fe(T-*p*-OMePP)(SH)]$^-$	0.444	0.024	−0.316	0.090	−0.203	0.181	0.122	−0.009	0.52	0.59	tw
[Fe(OEP)(2-MeIm$^-$)]$^-$	0.772	0.005	−0.511	0.497	−0.261	0.109	−0.090	0.032	0.56	0.65	48
[Fe(TpivPP)(2-MeIm$^-$)]$^-$	0.613	0.018	0.205	0.420	−0.365	−0.154	−0.012	−0.012	0.53	0.65	64
[Fe(TpivPP)(NO_3)]$^-$	0.574	0.012	−0.081	0.528	−0.207	−0.012	0.033	−0.001	0.55	0.65	63
[Fe(TpivPP)(O_2CCH_3)]$^-$	0.582	0.008	−0.077	0.505	−0.277	0.028	0.006	0.020	0.55	0.65	50
[Fe(TpivPP)(OC_6H_5)]$^-$	0.443	0.013	−0.058	0.387	−0.176	0.049	−0.100	0.003	0.57	0.63	46
[Fe(TpivPP)(SC_2H_5)]$^-$	0.542	0.017	0.228	0.396	−0.290	−0.018	0.018	−0.005	0.44	0.54	62
[Fe(TPP)(2-MeIm$^-$)]$^-$	0.666	0.005	−0.536	0.080	−0.301	0.019	−0.242	−0.016	0.56	0.66	48
[Fe(TPP)(Cl)]$^-$	0.649	0.009	−0.335	−0.359	−0.398	0.098	−0.106	−0.013	0.56	0.69	59

[a] Observed total distortion. [b] Mean deviations. [c] Displacement of iron from the mean plane of the four pyrrole nitrogen atoms. [d] Displacement of iron from the 24-atom mean plane.

Table 7. Selected Bond Distances and Angles for [Na(222)][Fe(Por)(SH)]

Por	Fe−N[a]	Fe−S[a]	S−H[a]	N−Fe−N[b]	Fe−S−H[b]
OEP, Fe(1)	2.1148(13)	2.3929(5)	1.31(2)	86.18(5)	98.8(12)
	2.1172(13)			86.15(5)	
	2.1219(13)			86.35(5)	
	2.1231(13)			86.65(5)	
OEP, Fe(2)	2.0976(13)	2.3830(5)	1.23(2)	87.50(5)	100.3(15)
	2.1073(14)			86.00(5)	
	2.1136(14)			86.47(5)	
	2.1138(14)			86.32(5)	
T-*p*-OMePP	2.105(3)	2.3887(13)	1.36(5)	86.61(12)	106.(2)
	2.105(3)			86.06(12)	
	2.108(3)			86.19(12)	
	2.116(3)			87.00(12)	

[a] Å. [b] deg.

than that in the OEP species, it is still strongly distorted, as shown in Table 6, with unusually large *wav*(*x*,*y*) components. A complete description of the treatment of hydrogen atoms of the HS^- ligand in the two complexes is given in the Supporting Information. A comparison of the Fe−S−H geometries with those of thiolates (Table 7) shows strong similarities.

Summary

This work clearly shows that HS^-, the most abundant form of H_2S at physiological pH, can act as a good ligand in iron porphyrinate systems and that the combination of heme proteins and the HS^- ligand could have a significant place in heme biological systems. The observed reducing power of HS^- with isolated hemes strongly suggests that heme proteins coordinating to sulfide ligands in the iron(III) oxidation state either must have specialized (low-polarity) environments or must allow only limited access to the HS^-/S^{2-} binding site. There are no equivalent restrictions for the iron(II) species. Solution UV−vis spectral investigations show stability for three distinct iron(II) species [Fe(Por)(SH)]$^-$, [Fe(Por)-(SH)$_2$]$^{2-}$, and a mixed-ligand species [Fe(Por)(SH)(Im)]$^-$. The five-coordinate species, [Fe(Por)(SH)]$^-$, are the first hydrosulfidoiron(II) porphyrinate compounds to be synthesized, isolated, and characterized by single-crystal structure determinations, IR and Mössbauer spectroscopy, and mass spectrometry. The results from all analyses are consistent with high-spin iron(II) with iron-bound sulfur. The physical properties are most similar to those of other high-spin iron(II) porphyrinates with axial anionic ligands. Solution binding studies yield values for formation constants that are comparable to those of imidazoles. Extinction coefficients and peak maxima for hydrosulfidometalloporphyrin complexes have been reported. Porphyrin core conformations for the [Fe(Por)(SH)]$^-$ species were analyzed by NSD and compared for all iron(II) species with anionic ligands. The OEP complexes may display larger contributions from doming than those of related iron(II) species.

Acknowledgment. We thank Prof. Ken Olson, Indiana University School of Medicine−South Bend, for early discussions on the potential gasotransmitter H_2S. We acknowledge Dr. W. C. Boggess of the University of Notre Dame for help with mass spectrometry. We thank the National Institutes of Health for support of this research under Grant GM-38401 and the NSF for X-ray instrumentation support under Grant CHE-0443233.

Supporting Information Available: Discussion of the hydrosulfide hydrogen atom assignment in the X-ray crystal structures, further validation of sulfur ligation, and experimental details of UV−vis binding studies, ORTEP drawing of anion **2** of [Na(222)]Fe(OEP)(SH)] (Figure S1), plot of the asymmetric unit of the structure for [Na(222)]Fe(OEP)(SH)]·0.5C_6H_6 (Figure S2), thermal ellipsoid plot for [Fe(T-*p*-OMePP)(SH)]$^-$ (Figure S3), UV−vis plot of the reactions of [Fe^{II}(TMP)] with HS^- (Figure S4), mean-plane diagrams for [Na(222)]Fe(OEP)-(SH)] (Figure S5), mean-plane diagrams for [Fe(T-*p*-OMePP)-(SH)]$^-$ (Figure S6), spectra detailing the reaction products with SH^- and Fe^{III} (Figure S7), complete crystallographic information for [Na(222)][Fe(OEP)(SH)]·0.5C_6H_6 (Tables S1−S6) and that for Na(222)][Fe(T-*p*-OMePP)(SH)]·C_6H_5Cl (Tables S7−S12), and crystallographic data in CIF format. This material is available free of charge via the Internet at http://pubs.acs.org.